Spin-freezing perspective on cuprates

Philipp Werner,[1] Shintaro Hoshino,[2] and Hiroshi Shinaoka[3]
[1]*Department of Physics, University of Fribourg, 1700 Fribourg, Switzerland*
[2]*RIKEN Center for Emergent Matter Science (CEMS), Wako, Saitama 351-0198, Japan*
[3]*Department of Physics, Saitama University, Saitama 338-8570, Japan*
(Received 2 August 2016; published 27 December 2016)

The high-temperature superconducting state in cuprates appears if charge carriers are doped into a Mott-insulating parent compound. An unresolved puzzle is the unconventional nature of the normal state above the superconducting dome and its connection to the superconducting instability. At weak hole doping, a "pseudogap" metal state with signatures of time-reversal symmetry breaking is observed, which near-optimal doping changes into a "strange metal" with non-Fermi-liquid properties. Qualitatively similar phase diagrams are found in multiorbital systems, such as pnictides, where the unconventional metal states arise from a Hund-coupling-induced spin freezing. Here, we show that the relevant model for cuprates, the single-orbital Hubbard model on the square lattice, can be mapped onto an effective multiorbital problem with strong ferromagnetic Hund coupling. The spin-freezing physics of this multiorbital system explains the phenomenology of cuprates, including the pseudogap, the strange metal, and the d-wave superconducting instability. Our analysis suggests that spin/orbital freezing is the universal mechanism which controls the properties of unconventional superconductors.

DOI: 10.1103/PhysRevB.94.245134

I. INTRODUCTION

Hund-coupling effects, in particular spin freezing [1], produce remarkable phenomena in correlated multiorbital systems [2]. The emergence of magnetic moments in the correlated metal phase leads to characteristic non-Fermi-liquid properties [1]. At low enough temperature, the fluctuating local moments can trigger a symmetry breaking to unconventional superconducting or excitonic states, which generically border a magnetically ordered phase [3,4]. The spin-freezing crossover occurs in a narrowly defined range of fillings and interaction strengths, and the remarkable fact is that many unconventional multiband superconductors fall into this parameter region. Examples are iron pnictides [5–8], chromium-based superconductors [9], strontium ruthenates [1,2,4], and uranium-based compounds [3]. In fulleride superconductors [10,11], where the effective Hund coupling is negative [12] and the roles of spin and orbital are in some sense exchanged, the unconventional superconducting state is associated with an orbital-freezing phenomenon [13]. A conspicuous exception from this almost exhaustive list of unconventional superconductors is the cuprates, which are typically discussed in terms of a single-band Hubbard model, where the Hund interaction does not appear.

Here, we introduce a basis transformation which maps the two-dimensional (2D) single-orbital Hubbard model onto a two-orbital model with ferromagnetic Hund coupling. The spin-freezing physics of this two-orbital system explains the pseudogap and bad-metal state of the weakly doped Hubbard model and the crossover to Fermi-liquid properties near optimal doping. We will also show that the slow local moment fluctuations associated with spin freezing provide the glue for d-wave pairing.

II. MODEL AND METHOD

We consider the 2D Hubbard model with on-site interaction U, nearest-neighbor hopping t, and next-nearest-neighbor hopping t',

$$\mathscr{H} = \sum_i U n_{i\uparrow} n_{i\downarrow} - \sum_i \mu(n_{i\uparrow} + n_{i\downarrow}) - t \sum_{\langle i,j\rangle,\sigma} (d^\dagger_{i\sigma} d_{j\sigma} + \text{H.c.}) - t' \sum_{\langle\langle i,j\rangle\rangle,\sigma} (d^\dagger_{i\sigma} d_{j\sigma} + \text{H.c.}). \tag{1}$$

Here, i and j are site indices, $\langle i,j\rangle$ denotes nearest-neighbor pairs, and $\langle\langle i,j\rangle\rangle$ next-nearest-neighbor pairs. The density operator is $n_\sigma = d^\dagger_\sigma d_\sigma$ and the chemical potential is μ. This model is a fundamental model of cuprate superconductors, since it describes the physics of the copper-oxygen plane. More specifically, the single band corresponds to the strongly hybridized antibonding combination of Cu $d_{x^2-y^2}$ and O p_x and p_y orbitals. A typical parameter choice is $U \approx 8t$ and $t' \approx -0.3t$ [14]. Since there is only a single orbital per site, Hund-coupling effects such as spin freezing have not been discussed in connection with cuprates.

Instead, because of the strong antiferromagnetic correlations and the d-wave nature of the superconducting state, the physics of the plaquette, illustrated in the left-hand panel of Fig. 1, plays a prominent role. This plaquette is the building block for 4-site cluster dynamical mean field theory (DMFT) calculations [15,16], which have been extensively used to investigate the 2D Hubbard model and which have produced phase diagrams in qualitative agreement with that of cuprates [17].

To analyze the physics of the plaquette and the 2D Hubbard model from a multiorbital perspective, we perform a basis transformation to bonding/antibonding orbitals, as illustrated in Fig. 1. If the sites are numbered in an anticlockwise fashion starting from the bottom left, the transformed orbitals are

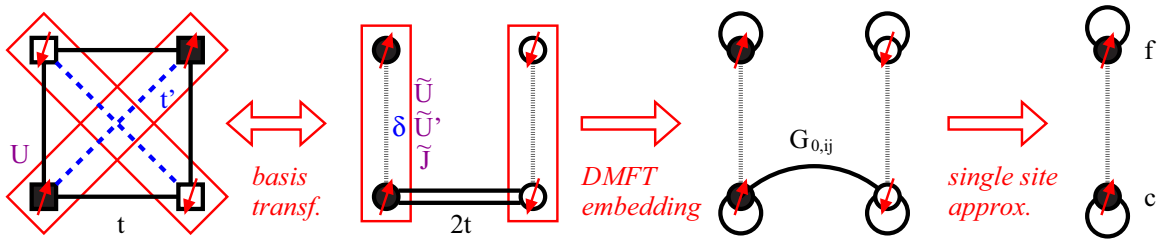

FIG. 1. Illustration of the mapping of the plaquette with nearest-neighbor hopping t and diagonal hopping t' onto a coupled pair of two-orbital models. If U is the on-site interaction on the plaquette, the two-orbital system has a Slater-Kanamori type interaction with $\tilde{U} = \tilde{U}' = \tilde{J} = U/2$. The diagonal hopping translates into a crystal-field splitting $\delta = 2t'$. The third panel shows the self-consistent embedding of the two-orbital system into a noninteracting bath described by $(G_0)_{ij}$, and the rightmost panel the simplification to a single-site two-orbital impurity problem.

defined as follows:

$$c_1 = \frac{1}{\sqrt{2}}(d_1 + d_3), \quad c_2 = \frac{1}{\sqrt{2}}(d_2 + d_4), \tag{2}$$

$$f_1 = \frac{1}{\sqrt{2}}(d_1 - d_3), \quad f_2 = \frac{1}{\sqrt{2}}(d_2 - d_4). \tag{3}$$

This transformation maps the plaquette onto a pair of two-orbital systems, with a hopping of $2t$ between the antibonding (c) orbitals and no hopping between the bonding (f) orbitals. The interactions between the two orbitals on a given site are of the "Slater-Kanamori" type,

$$\begin{aligned}\tilde{\mathscr{H}}_{\rm loc} = &\sum_{\gamma=c,f} \{\tilde{U} n_{\gamma\uparrow} n_{\gamma\downarrow} - [\mu + (-1)^\gamma t'](n_{\gamma\uparrow} + n_{\gamma\downarrow})\} \\ &+ \sum_{\sigma} [\tilde{U}' n_{c\sigma} n_{f\bar{\sigma}} + (\tilde{U}' - \tilde{J}) n_{c\sigma} n_{f\sigma}] \\ &- \tilde{J}[c^\dagger_\downarrow f^\dagger_\uparrow f_\downarrow c_\uparrow + f^\dagger_\uparrow f^\dagger_\downarrow c_\uparrow c_\downarrow + \text{H.c.}],\end{aligned} \tag{4}$$

but with unconventional parameters $\tilde{U} = \tilde{U}' = \tilde{J} = U/2$ [18]. In particular, the ferromagnetic Hund-coupling parameter $\tilde{J}$ of these two-orbital systems is very large. The effect of the diagonal hopping t' is to produce a chemical potential shift $\Delta\mu = \pm t'$ for the c and f orbitals, i.e., a crystal-field splitting of $\delta = 2t'$ in the two-orbital model language. In $\tilde{\mathscr{H}}_{\rm loc}$, $(-1)^\gamma = 1$ for the c orbital and -1 for the f orbital.

In cluster DMFT (CDMFT) [15], the plaquette is coupled to a self-consistently determined bath of noninteracting electrons, which mimics the effect of the intercluster hopping processes. The Weiss Green's function G_0 is the Green's function of the noninteracting embedded plaquette, and by virtue of the DMFT construction [19] describes the propagation via intracluster and intercluster hoppings. Due to the symmetries of the plaquette (refer to the Appendix), the only nonzero elements are $(G_0)_{c_i c_j}$ $(i \neq j)$ and the on-site terms $(G_0)_{c_i c_i}$ and $(G_0)_{f_i f_i}$ $(i = 1,2)$, as shown in the third panel. [The $(G_0)_{f_i f_i}$ elements originate from the intracluster hopping in the transformed basis.]

The structure of G_0 suggests a single-site DMFT approximation based on a two-orbital model, as sketched in the right-hand panel of Fig. 1. We thus end up with an effective description in terms of

$$\begin{aligned}\mathscr{H}_{\rm 2orbital} = &- \tilde{t}_c \sum_{\langle i,j\rangle,\sigma} (c^\dagger_{i,\sigma} c_{j,\sigma} + \text{H.c.}) \\ &- \tilde{t}_f \sum_{\langle i,j\rangle,\sigma} (f^\dagger_{i,\sigma} f_{j,\sigma} + \text{H.c.}) + \sum_i \tilde{\mathscr{H}}_{{\rm loc},i},\end{aligned} \tag{5}$$

with the local part of the Hamiltonian defined in Eq. (4) and $\tilde{t}_c$, $\tilde{t}_f$ appropriate hopping amplitudes for the c and f electrons. To obtain realistic values for the hopping parameters, we calculated the local density of states (DOS) for the c and f electrons from the CDMFT solution of the noninteracting model; see Fig. 2. If $t' = 0$ [panel (a)], the square root of the variance is $2.45t$ for the c-DOS and $1.41t$ for the f-DOS. For $t' = -0.3t$ [panel (b)], the f-DOS is shifted down, while the c-DOS is shifted up.

Because single-site DMFT simulations produce the generic behavior of a high-dimensional system irrespective of the details of the DOS, we can further simplify the problem by choosing semicircular DOS with the proper bandwidth (W) ratio $W_c/W_f = 1.74$. For this choice of DOS, the DMFT self-consistency condition becomes $\Delta_{\gamma\gamma} = (W_\gamma/4)^2 G_{\gamma\gamma}$ $(\gamma = f,c)$, where the hybridization function Δ is related to the Weiss Green's function G_0 by $G^{-1}_{0,\gamma\gamma}(i\omega_n) = i\omega_n + \mu - \Delta_{\gamma\gamma}(i\omega_n)$ [19]. We solve the DMFT equations using the matrix version [20] of the hybridization expansion continuous-time Monte Carlo technique [21] and use $W_c \equiv W$ as the unit of energy.

III. SPIN FREEZING AND NON-FERMI-LIQUID METAL

The emergence of frozen local moments in multiorbital models with Hund coupling profoundly affects the metal state close to the half-filled Mott insulator [1]. It is therefore interesting to explore the properties of model (5) as one dopes this system away from the half-filled Mott insulator. We first discuss the results obtained for the semicircular DOS and $\delta = 0$. To work in the relevant interaction regime of the two-orbital system, we choose $U/W = 1.25$, which is somewhat larger than the Mott critical value $U_c/W = 0.98$ (1.03) of the half-filled system at inverse temperature $\beta W = 200$ (800).

Since spin-freezing physics leaves clear traces in the frequency dependence of the self-energy [1] it is instructive to analyze the doping evolution of the self-energies. Figure 3(a) plots $-\text{Im}\Sigma_{ff}(i\omega_n)$ for different fillings and temperatures. Let us characterize the low-frequency behavior by the fit

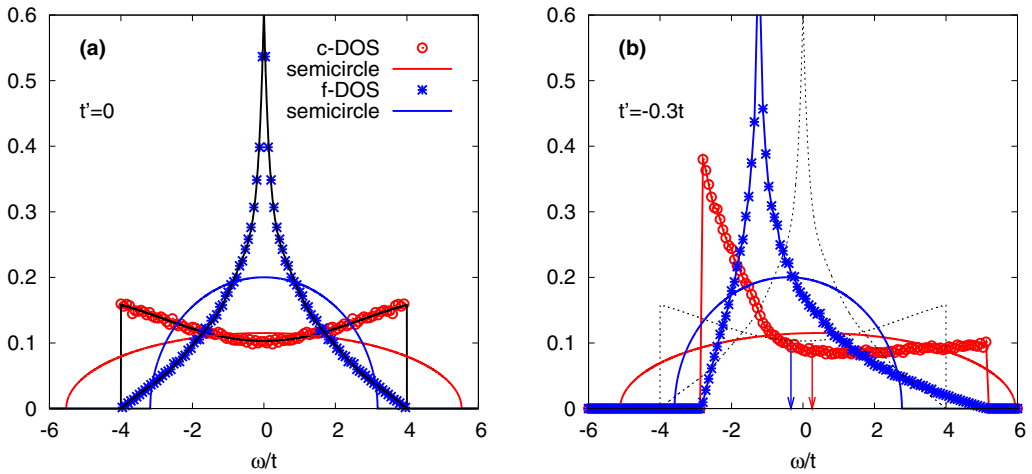

FIG. 2. Noninteracting DOS for the c and f electrons extracted from a noninteracting plaquette CDMFT calculation (symbols) and semicircular DOS with identical variance. (a) Model with $t' = 0$. Black lines show the fit functions used in the realistic-DOS simulations. (b) Realistic DOS for the model with $t' = -0.3t$ (symbols) and semicircular DOS with a crystal-field splitting $\delta = 0.075W$. The arrows indicate the centers of the bands at energy $-0.34t$ and $0.26t$, respectively.

$\mathrm{Im}\,\Sigma(\mathrm{i}\omega_n) = b(\omega_n)^\alpha$. The doping-dependent exponents α, displayed in Fig. 3(b), exhibit a minimum near half filling, which we use to define the boundary of the spin-frozen regime. The minimum appears because the self-energy in the spin-frozen regime shows a more linear frequency dependence, similar to a Mott insulator with chemical potential away from the particle-hole symmetric value. At low temperatures, this definition of the spin-frozen regime somewhat underestimates its extent compared to the definition based on the fitting function $c + b(\omega_n)^\alpha$ [1], but this detail is not important for the following discussion.

In the semicircle DOS calculations, the exponents extracted from the c- and f-electron self-energies are similar, with somewhat enhanced spin-freezing effects for f. Stable local moments exist only in a rather narrow doping range of a few percent. Within single-site DMFT, this doping range increases slightly with increasing temperature. We can also roughly determine the doping range associated with the bad-metal state by using the criterion $\alpha < 0.5$ for the incoherent region. The spin-freezing and bad-metal crossover lines are indicated by dashed black lines with open and full circles in the temperature-filling phase diagram of Fig. 4(a), where we assumed a bandwidth of 2 eV (relevant for La_2CuO_4 [22]), to translate temperature into K.

The single-site DMFT analysis demonstrates that our effective 2-orbital model, despite the modified Slater-Kanamori interaction with $\tilde{U} = \tilde{U}'$, the unusually large value of $\tilde{J} = \tilde{U}$, and the different bandwidths for the c and f electrons, exhibits the characteristic spin-freezing behavior and non-Fermi-liquid properties expected for multiorbital systems in the vicinity of the half-filled Mott insulator [1,4,7,23,24]. Going back from the c/f- to the original d-fermion description, it follows that the freezing of a composite spin formed on diagonally opposite sites of the plaquette is a fundamentally important

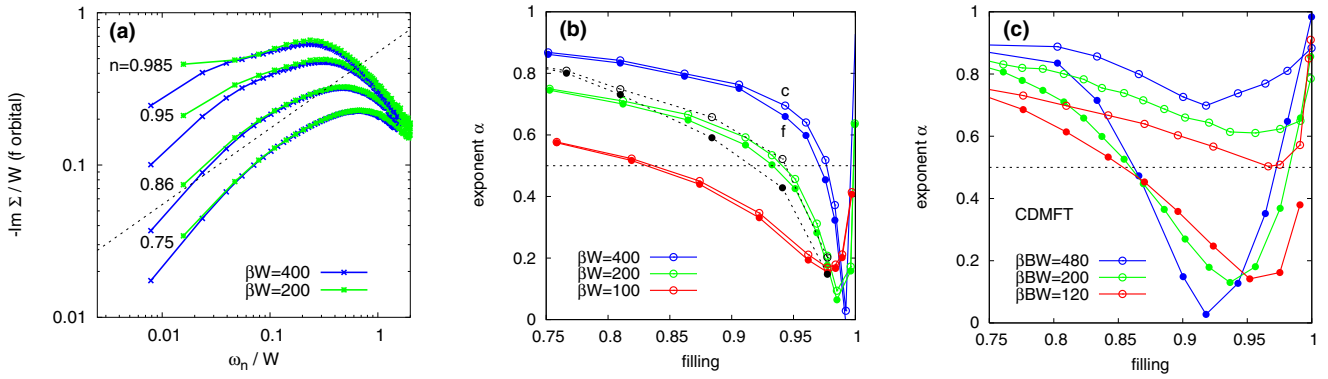

FIG. 3. Doping dependence of the self-energy revealing the non-Fermi-liquid behavior and spin-freezing crossover. (a) f-electron self-energies for $U/W = 1.25$, $\delta = 0$ and indicated inverse temperatures β. The low-frequency behavior of the self-energy indicates a crossover to a spin-frozen state around filling $n = 0.98$ at the higher temperature. The black dashed line is proportional to $(\omega_n)^{1/2}$. (b) Exponents α extracted from the fits $-\mathrm{Im}\Sigma(i\omega_n) = b(\omega_n)^\alpha$ at the lowest two Matsubara frequencies. Both the results for the f (full symbols) and c electron (open symbols) are shown. For comparison, we also plot by dashed black lines the exponents obtained for the calculation with realistic DOS at $\beta W = 240$. (c) Analogous exponents extracted from the CDMFT calculation.

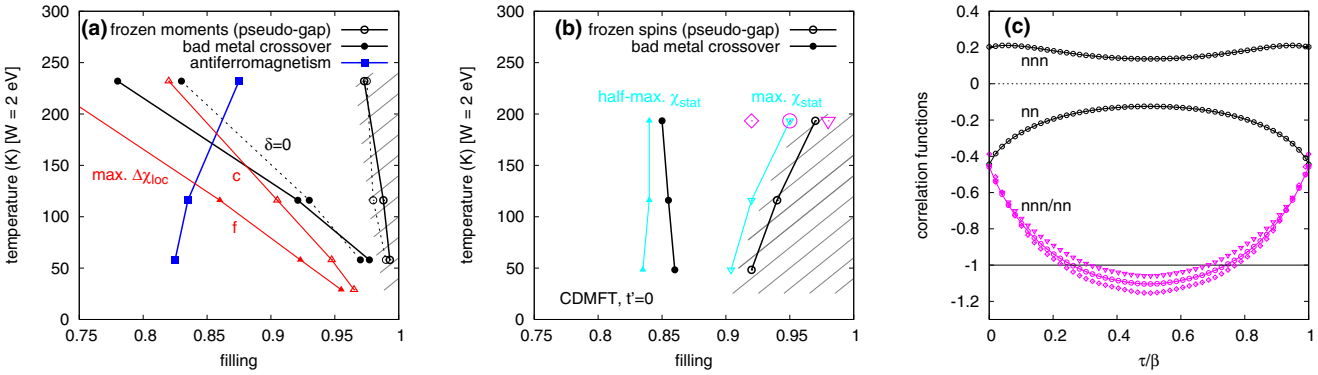

FIG. 4. Phase transitions and crossover lines in the doping-temperature phase diagram. Here, we assume a bandwidth of 2 eV to translate the temperature into K. (a) Results from single-site DMFT simulations of the effective 2-orbital model with solid lines corresponding to $\delta = 0.075W$ and dashed lines to $\delta = 0$. (b) Crossover lines extracted from the behavior of the f-electron self-energy (black) and f-electron S_z-S_z correlation function (light blue) in CDMFT. For three fillings near the spin-freezing line (pink symbols) we plot the ratio of next-nearest-neighbor (nnn) and nearest-neighbor (nn) d-electron S_z-S_z correlations in (c). The nn and nnn curves are multiplied by a factor of 4 for better visibility.

phenomenon in the 2D single-band Hubbard model (1) and, hence, in cuprates. As illustrated in Fig. 1, the formation of this composite spin corresponds to the appearance of ferromagnetic correlations on next-nearest-neighbor sites.

Let us comment on the quantitative effects of the realistic DOS. As shown in Fig. 2, the realistic f-DOS has a sharp peak at $\omega = 0$, which enhances the relative number of holes doped into the f orbitals, especially at larger dopings. It also considerably increases the value of U_c/W from $\approx$1 in the semicircle case to about 1.5. Despite these quantitative changes, the spin-freezing behavior near the half-filled Mott insulator is qualitatively the same as in the semicircle DOS simulation. To demonstrate this, we also plot the exponents α extracted from realistic-DOS simulations with $U = 14t$ ($U = 1.75W$) and $\beta t = 30$ ($\beta W = 240$) in Fig. 3(b) (dashed black lines).

We will next consider the model with $t' = -0.3t$. This diagonal hopping translates into a crystal-field splitting $\delta = 2t'$ which pushes the f band down [see Fig. 2(b)]. Since $0.6t$ corresponds to 0.075 times the bandwidth of the model with $t' = 0$, we use such a splitting in the calculations with semicircular DOS. The corresponding spin-freezing line is shown in Fig. 4(a) by a solid black line with full dots, while the bad-metal crossover defined by $\alpha = 0.5$ is indicated by the solid black line with open dots. It turns out that the crystal-field splitting does not qualitatively change the crossover lines in the temperature-filling phase diagram.

The bad-metal behavior originates from Hund-coupling-induced local moments. In Fig. 5(a) we plot the dynamical contribution to the local spin susceptibility, $\Delta\chi_{\rm loc}^{(c,f)} = \int_0^\beta d\tau\, S_{\rm dyn}^{(c,f)}(\tau)$ with

$$S_{\rm dyn}^{(c,f)}(\tau) \equiv \left\langle S_z^{(c,f)}(\tau) S_z^{(c,f)}(0)\right\rangle - \left\langle S_z^{(c,f)}(\beta/2) S_z^{(c,f)}(0)\right\rangle, \quad (6)$$

for different temperatures and dopings. The local spin fluctuations are strongly enhanced near the spin-frozen regime at low temperature. The peak values define the crossover lines which are plotted in red in Fig. 4(a). The comparison to the crossover line derived from the self-energy suggests that the non-Fermi-liquid properties are caused by the slowly fluctuating local moments in the spin-freezing crossover regime. As these moments freeze below a doping concentration of a few percent, the low-energy single-particle spectral weight is strongly reduced, and a narrow pseudogap opens [see Fig. 5(c)] [25]. The size of the pseudogap appears to be related to the characteristic energy of the local spin fluctuations. As shown in Fig. 5(b), $\mathrm{Im}S_{\rm dyn}^{(c,f)}(\omega)$ exhibits a peak near $\omega \approx 0.01W$ in the low-doping regime.

Experimentally, it is known that the normal-state pseudogap region in cuprates can be enhanced by adding magnetic impurities [26]. Ellipsometry measurements showed that the addition of Ni^{2+} impurities with spin $S = 1$ strengthen the Cu spin correlations and induce a bulk spin-freezing transition even at optimal doping. This points to an important role of magnetic correlations in the formation of the pseudogap and is consistent with our spin-freezing scenario, since the static Ni^{2+} moments will influence the slowly fluctuating composite spins in the spin-freezing crossover region and (at large enough impurity concentration) lock them into a spin-frozen state.

IV. SYMMETRY BREAKING AND SHORT-RANGE CORRELATIONS

It is interesting to consider also the instabilities to long-range orders and the effect of short-range correlations. Ordering instabilities can be detected by computing the corresponding lattice susceptibilities, based on a DMFT estimate of the local vertex and a solution of the Bethe-Salpeter equation [3,4]. In the calculations with semicircle DOS and crystal-field splitting, antiferromagnetic order is stable at low temperature up to about 18% hole doping [Fig. 4(a)]. As expected, the order is overestimated compared to CDMFT simulations, which account for spatial fluctuations. For $U = 8t$ and $t' = -0.3t$, 4-site CDMFT yields antiferromagnetic order up to 13% hole doping [27], but it was also shown that the stability region depends sensitively on details of the band structure.

Recent studies of two-orbital models with crystal-field splitting revealed an instability to spin-orbital order [4,28], which is intricately connected to spin freezing. In models with Ising-type interactions spin-orbital order characterized by a nonzero expectation value of the operator $o_i^{xx} =$

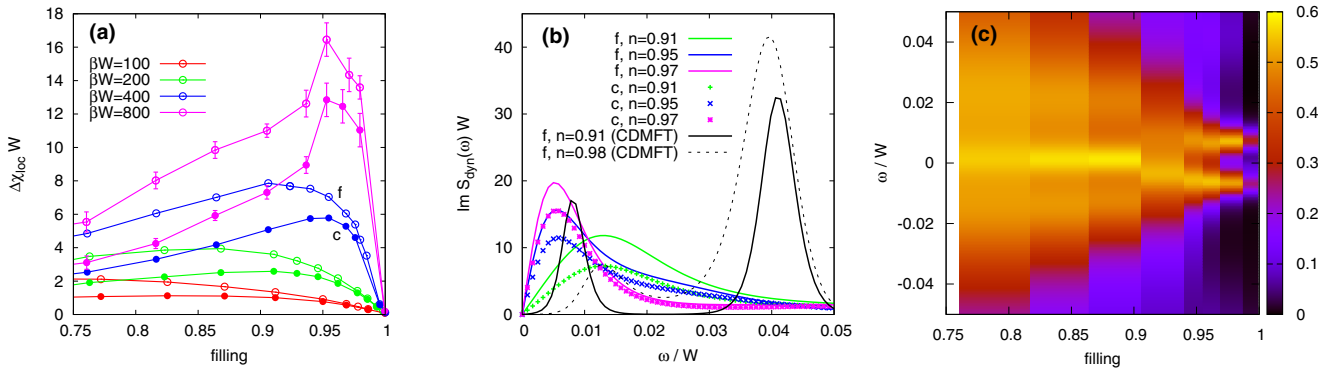

FIG. 5. Local spin susceptibility and single-particle spectral function. (a) Dynamical contribution to $\chi_{\rm loc}^{(c,f)}$ as a function of filling for indicated values of the inverse temperature. (b) Spectral function of the dynamical contribution to the spin-spin correlation function, obtained by maximum entropy analytical continuation [37,38], for $\beta W = 400$ and different fillings. (c) Doping evolution of the f-electron single-particle spectral function at $\beta W = 400$. (2-orbital results for $\delta = 0.075W$, CDMFT results for $t' = 0$ and $\beta W = 480$.)

$\sum_{\gamma,\gamma'=c,f} \sum_{\sigma,\sigma'} \gamma_{i\sigma}^{\dagger} \sigma^x_{\gamma\gamma'} \sigma^x_{\sigma\sigma'} \gamma'_{i\sigma'}$ can exist beyond the stability region of the antiferromagnet (σ^x denotes a Pauli matrix) [4]. In the presence of spin-flip and pair-hopping terms, our techniques do not allow us to search for this ordering instability. Nevertheless, it is interesting to note that after the transformation back to the d basis, o^{xx} maps onto antiferromagnetic order with ordering vector $\boldsymbol{q} = (0,\pi)$, represented by $\sum_{\sigma\sigma'} \sigma^x_{\sigma\sigma'} (d^{\dagger}_{1\sigma} d_{1\sigma'} + d^{\dagger}_{2\sigma} d_{2\sigma'} - d^{\dagger}_{3\sigma} d_{3\sigma'} - d^{\dagger}_{4\sigma} d_{4\sigma'})$. It is degenerate with the y,z components by SU(2) symmetry and with the $\boldsymbol{q} = (\pi,0)$ ordering vector by 90° rotation symmetry. Remarkably, *short-ranged* order of this type has been detected experimentally in cuprates upon entering the pseudogap phase [29,30].

There is also evidence from polarized neutron scattering experiments for some kind of intraplaquette magnetic order and time-reversal symmetry breaking in the pseudogap regime [31,32]. While this observation has been mainly discussed in connection with the possible appearance of current loops [33], there are inconsistencies between the latter theory and the experiments concerning the orientation of the moments. The alignment and freezing of the spins on diagonally opposite corners of the plaquette provides an alternative explanation, since it breaks time-reversal symmetry on short time and length scales, and reduces the 90° rotation symmetry to a mirror symmetry. This mechanism does not *a priori* favor any particular direction of the moments.

Of course, in the 2D Hubbard model, antiferromagnetic correlations and nearest-neighbor singlet formation are important and change the single-site DMFT results to some extent. To capture these effects one would have to implement a 2-site CDMFT calculation of the 2-orbital system (see second panel of Fig. 1). With a proper lattice embedding, such a simulation would be exactly equivalent to the plaquette CDMFT in the original d basis. Hence, in order to address the effect of short-range correlations, we will now discuss CDMFT simulation results transformed into the c/f basis, focusing on $U = 8t$ and $t' = 0$. The CDMFT simulations are performed with improved Monte Carlo updates [34], in a single-particle basis which diagonalizes the intraplaquette hopping. For better statistics, the correlation functions are measured in the d basis using a worm-sampling algorithm [35,36].

As illustrated in Fig. 3(c), the nonlocal correlations result in a stronger differentiation between the c- and f-electron self-energies, with the latter exhibiting much more pronounced non-Fermi-liquid effects and a substantially lower "Kondo screening" temperature. The second, quite expected, difference concerns the temperature dependence of the spin-freezing and bad-metal crossover lines. In single-site DMFT, these crossover lines have a negative slope in the temperature-filling phase diagram, because disordered local moments have a large entropy. If intersite correlations are taken into account, the frozen moments can form singlet states with a low entropy. As a result of this, the frozen moment regime (hashed region) determined from the minimum of the f-electron exponent α increases with decreasing temperature in the CDMFT solution. Similarly, the bad-metal crossover line determined by the exponent $\alpha = 0.5$ is now almost vertical in the temperature-filling phase diagram. The CDMFT crossover lines for $t' = 0$ are illustrated in Fig. 4(b).

The pseudogap regime of the CDMFT solution can still be associated with frozen f moments, as evidenced by a maximum in $\chi_{\rm stat}^{(f)} = \beta \langle S_z^{(f)}(\beta/2) S_z^{(f)}(0) \rangle$ near the spin-freezing crossover line, while the bad-metal crossover near optimal hole doping is related to the emergence of local moments [the light blue line with solid triangles in Fig. 4(b) indicates the doping where $\chi_{\rm stat}^{(f)}$ reaches half of the maximum value].

The main qualitative difference to the single-site 2-orbital simulations is that $\chi_{\rm loc}^{(f)}$ decreases as one moves deeper into the spin-frozen regime as a result of singlet formation (overestimated in the 2×2 geometry due to the dominance of the "plaquette singlet state" [39]), and hence that $\Delta\chi_{\rm loc}$ ceases to be a good measure of the fluctuations of the composite spin in the underdoped regime. To directly demonstrate the presence of robust ferromagnetic correlations along the diagonal of the plaquette we plot the nearest-neighbor and next-nearest-neighbor spin correlations near the spin-frozen regime in the original d basis [see Fig. 4(c)]. While antiferromagnetic nearest-neighbor correlations are dominant at short times, the ferromagnetic next-nearest-neighbor correlations decay more slowly and eventually exceed the antiferromagnetic ones.

We have also calculated $S_{\rm dyn}^{(f)}(\omega)$ from the CDMFT solution and found the same low-energy peak near $\omega \approx 0.01W$ as

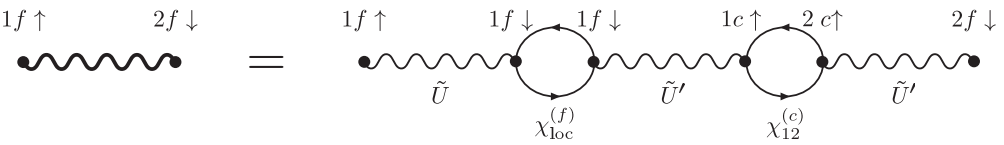

FIG. 6. Illustration of the lowest-order diagram which generates an attractive interaction between $(1, f, \uparrow)$ and $(2, f, \downarrow)$.

in the single-site 2-orbital model [Fig. 5(b), black lines]. However, there is now also a second mode with an energy $\approx 0.04W$, which is related to antiferromagnetic fluctuations. In the spin-freezing crossover regime, both modes are present. In the spin-frozen (pseudogap) regime, the lower-energy peak associated with f-moment fluctuations disappears, while the peak associated with antiferromagnetic fluctuations gains weight.

V. SUPERCONDUCTIVITY

We finally address the question of superconductivity and possible connections to spin freezing. The 4-site CDMFT solution of the doped Hubbard model has been shown to exhibit d-wave superconductivity [15], and we thus expect to find this ordered state in a 2-site cluster DMFT simulation of the 2-orbital model. Recent DMFT simulations on larger clusters revealed a sharp low-energy peak at $\omega \approx 0.013W$ in the imaginary part of the anomalous self-energy [40]. This energy agrees remarkably well with the characteristic energy of the local spin fluctuations, observed in both the single-site DMFT simulation of the effective 2-orbital model and in the plaquette CDMFT solution [Fig. 5(b)]. This strongly suggests that the enhanced local moment fluctuations in the crossover regime to the spin-frozen state play a role in the formation of the d-wave superconducting state.

To get some clues of the possible mechanism let us first transform the d-wave order parameter $(d^\dagger_{1\uparrow}d^\dagger_{2\downarrow} - d^\dagger_{1\downarrow}d^\dagger_{2\uparrow}) - (d^\dagger_{2\uparrow}d^\dagger_{3\downarrow} - d^\dagger_{2\downarrow}d^\dagger_{3\uparrow}) + (d^\dagger_{3\uparrow}d^\dagger_{4\downarrow} - d^\dagger_{3\downarrow}d^\dagger_{4\uparrow}) - (d^\dagger_{4\uparrow}d^\dagger_{1\downarrow} - d^\dagger_{4\downarrow}d^\dagger_{1\uparrow})$ to the c/f basis. The resulting expression is remarkably simple and suggestive:

$$2(f^\dagger_{1\uparrow}f^\dagger_{2\downarrow} - f^\dagger_{1\downarrow}f^\dagger_{2\uparrow}), \tag{7}$$

where the indices 1 and 2 now refer to the two sites of the two-orbital cluster in the second panel of Fig. 1. It thus remains to be shown how local spin fluctuations can induce an effective attraction between the f electrons with opposite spins on neighboring sites.

In a weak-coupling picture [3,41] the effective interaction $\tilde{U}^{\rm eff}_{\alpha,\beta}$ between two flavors $\alpha,\beta = (i,\gamma,\sigma)$, which takes into account simple bubble diagrams, can be obtained from the solution of the equation $\tilde{U}^{\rm eff}_{\alpha\beta} = \tilde{U}_{\alpha\beta} - \sum_{\alpha_1\beta_1}\tilde{U}_{\alpha\alpha_1}\chi_{\alpha_1\beta_1}\tilde{U}^{\rm eff}_{\beta_1\beta}$. This indeed yields an attraction

$$\tilde{U}^{\rm eff}_{(1,f,\uparrow),(2,f,\downarrow)} = 2\tilde{U}^3\chi^{(f)}_{\rm loc}\chi^{(c)}_{12} + O(\tilde{U}^5) \tag{8}$$

between $f_{1,\sigma}$ and $f_{2,\bar{\sigma}}$ which becomes stronger with increasing $\chi^{(f)}_{\rm loc} \equiv \Delta\chi^{(f)}_{\rm loc}$ (in the weak-coupling regime, there are no frozen moments). Note that $\chi^{(c)}_{12} = -\int_0^\beta d\tau G_{c,12}(\tau)G_{c,21}(-\tau) < 0$, while $\chi^{(f)}_{\rm loc} > 0$.

To understand the physical mechanism, it is instructive to look at the lowest-order diagram which contributes to $\tilde{U}^{\rm eff}_{(1,f,\uparrow),(2,f,\downarrow)}$ (Fig. 6). Because of $\tilde{U}' = \tilde{J}$, the interorbital same-spin interaction vanishes on each site, so the c-f interaction lines appearing in the diagram correspond to the interactions $(1,f,\sigma)$-$(1,c,\bar{\sigma})$ and $(2,c,\sigma)$-$(2,f,\bar{\sigma})$ (see also Fig. 1). Since the hopping between the sites conserves spin, the interaction between the sites is mediated by a bubble $\chi^{(c)}_{12}$. To connect $(1,c,\uparrow)$ to $(1,f,\uparrow)$, we have to insert a second bubble $\chi^{(f)}_{\rm loc}$. This is how the local f-spin susceptibility enters the calculation, and how the enhanced local spin fluctuations increase the effective attraction between the f electrons in the weak-coupling approach with bubble diagrams. We note that the contributions to $\chi_{\rm loc}$ include both the spin and charge parts, but as the interaction strength is increased, the spin contribution will dominate.

A numerical evaluation of the lowest-order diagram using the CDMFT data shows that the attractive interaction grows with decreasing temperature, and, even more interestingly, that it starts to grow substantially with decreasing doping around 20% doping. This is in good agreement with the CDMFT phase diagram [15], which exhibits a superconducting dome up to about 20% doping, and provides further support for our spin-freezing mechanism. Both the $\chi^{(c)}_{12}$ and $\chi^{(f)}_{\rm loc}$ fluctuations contribute to this growing attractive interaction. While $|\Delta\chi^{(c)}_{12}|$ grows more rapidly with decreasing doping, the value of $\Delta\chi^{(f)}_{\rm loc}$ is roughly a factor of two larger.

Up to this point, our argument has only taken into account the density-density interactions. To understand why the singlet form of the order parameter is stabilized [Eq. (7)], we have to consider the effect of the spin-flip term.

VI. DISCUSSION AND CONCLUSIONS

Starting from a transformation of the 4-site Hubbard plaquette to a bonding/antibonding basis, we have derived an effective description of the 2D Hubbard model in terms of a two-orbital system with "Slater-Kanamori" interaction and (for $t' \neq 0$) a crystal-field splitting. This model can be solved approximately within single-site DMFT, which leads to interesting new perspectives on the normal-state properties of the Hubbard model, and hence cuprates. In particular, the two-orbital model, which features a large ferromagnetic Hund coupling, exhibits a spin-freezing crossover in the vicinity of the half-filled Mott-insulating state. Our results suggest that optimally doped cuprates, like essentially all unconventional multiband superconductors, are located in a filling and interaction regime where the normal-state properties at elevated temperature are strongly influenced by the spin-freezing phenomenon. Spin/orbital freezing thus appears to be a universal mechanism underlying the physics of (at first sight) very diverse families of unconventional superconductors, including cuprates, pnictides, ruthenates, and fulleride- and uranium-based superconductors. Specifically, for the case of

cuprates, our analysis suggests that the enhanced fluctuations of a composite spin, consisting of aligned moments on diagonally opposite corners of a plaquette, produce the non-Fermi-liquid properties above the superconducting dome, while the freezing of these composite spins at weaker doping results in the pseudogap phase. It is interesting to note that the spin-freezing scenario does not involve a quantum critical point since spin-freezing exists only above a certain (doping-dependent) "Kondo screening" temperature.

Because the spin-frozen (pseudogap) state has suppressed local spin fluctuations, it is not amenable to superconductivity. In this sense, the freezing of the spins competes with superconductivity. On the other hand, the strongly and slowly fluctuating local moments in the spin-freezing crossover regime induce the superconducting instability and provide the glue for the d-wave pairing. It is also worthwhile to note that spin-freezing only appears at interactions $\gtrsim U_c$, i.e., in doped Mott insulators [1,6,7,42]. Our proposed mechanism thus requires that the parent compound, which in the case of the cuprates is the half-filled system, is in or close to the Mott regime.

Finally, let us comment on the relationship between our work and previous studies which emphasized similarities in the phase diagrams of cuprates and Hund metals such as iron pnictides. Ishida and Liebsch [6,7] first pointed out that if the "doping" of iron pnictides is measured relative to the half-filled state, the phase diagram exhibits the same sequence of paramagnetic phases as found in cuprates, namely Mott insulator to bad metal to Fermi-liquid metal. In both materials, the crossover to the Fermi-liquid state occurs at roughly 20% doping [6]. They also noted that the 4-site impurity problem of plaquette DMFT, if transformed into the diagonal cluster momentum basis, becomes a complicated multiorbital problem [43], which suggests a connection between Hund-coupling phenomena in multiband materials and the momentum-differentiation found in CDMFT studies of the 2D Hubbard model [27,39,44,45].

The diagonal cluster momentum basis considered in the work of Ishida and Liebsch, and also in related studies by de' Medici and co-workers [46], is complementary to the bonding/antibonding basis considered in this paper. While the numerical results of plaquette CDMFT do not depend on the cluster basis, as long as the impurity model is solved exactly and the lattice embedding is implemented correctly, a suitable choice of basis helps to reveal the underlying physics of correlation and crossover phenomena. The main advantages of the bonding/antibonding basis introduced here are the following: (i) The cluster problem is mapped to a multiorbital system with a standard Slater-Kanamori interaction (albeit with unusual parameters $\tilde{U} = \tilde{U}' = \tilde{J}$), which allows us to discuss the physics in terms of the spin-freezing phenomena that have been extensively investigated for such models over the past years. (ii) The d-wave superconducting order parameter maps to a simple nearest-neighbor singlet pairing of the f electrons, which also allows us to connect the superconducting instability to the spin-freezing crossover. (iii) The structure of the two-site cluster impurity problem enables the formulation of a single-site two-orbital DMFT approximation, and thus to disentangle the effect of spin freezing (local fluctuations of the composite spin) from the effect of short-range antiferromagnetic fluctuations.

Working out the precise connection between the freezing of composite spins on next-nearest-neighbor sites revealed by the bonding/antibonding basis and the momentum-selective behavior found in the diagonal basis is an interesting topic for future investigations, as is the possible connection between our single-site two-orbital description and the so-called valence-bond DMFT [47].

ACKNOWLEDGMENTS

The calculations were run on the Brutus cluster at ETH Zurich and the facilities of the Supercomputer Center at the Institute for Solid State Physics, University of Tokyo, using codes based on ALPS [48] and ALPSCore [36]. We thank C. Bernhard for interesting discussions, and L. Boehnke for providing the maximum entropy code for the analytical continuation of the spin-spin correlation functions. H.S. was supported by JSPS KAKENHI Grants No. 16H01064 (J-Physics) and No. 16K17735. P.W. acknowledges the hospitality of the Aspen Center for Physics and funding from FP7 ERC Starting Grant No. 278023.

APPENDIX: STRUCTURE OF THE WEISS GREEN'S FUNCTION AND THE HYBRIDIZATION FUNCTION

If the hybridization function and the Weiss Green's function of the standard plaquette CDMFT are transformed to the f/c basis, the only nonzero off-diagonal elements are those shown in the third panel of Fig. 1.

This may be understood as follows. The Green's function at each time and for each spin sector can be represented as a 4×4 matrix with the following structure:

$$\begin{pmatrix} \alpha & \beta & \gamma & \delta \\ \beta & \alpha & \beta & \gamma \\ \gamma & \beta & \alpha & \beta \\ \beta & \gamma & \beta & \alpha \end{pmatrix}, \tag{A1}$$

where α, β, γ, δ are numbers. In the f/c basis, the above matrix is transformed to

$$\begin{pmatrix} \alpha+\gamma & 0 & 2\beta & 0 \\ 0 & \alpha-\gamma & 0 & 0 \\ 2\beta & 0 & \alpha+\gamma & 0 \\ 0 & 0 & 0 & \alpha-\gamma \end{pmatrix}, \tag{A2}$$

where the order of the orbitals is $\{1c, 1f, 2c, 2f\}$. In (A2) we recognize the same structure as illustrated in the third panel of Fig. 1. The same argument applies to the hybridization function.

[1] P. Werner, E. Gull, M. Troyer, and A. J. Millis, Spin Freezing Transition and Non-Fermi-Liquid Self-Energy in a Three-Orbital Model, Phys. Rev. Lett. **101**, 166405 (2008).

[2] A. Georges, L. d. Medici, and J. Mravlje, Strong correlations from Hund's coupling, Annu. Rev. Condens. Matter Phys. **4**, 137 (2013).

[3] S. Hoshino and P. Werner, Superconductivity from Emerging Magnetic Moments, Phys. Rev. Lett. **115**, 247001 (2015).

[4] S. Hoshino and P. Werner, Electronic orders in multiorbital Hubbard models with lifted orbital degeneracy, Phys. Rev. B **93**, 155161 (2016).

[5] K. Haule and G. Kotliar, Coherence-incoherence crossover in the normal state of iron oxypnictides and importance of Hund's rule coupling, New J. Phys. **11**, 025021 (2009).

[6] H. Ishida and A. Liebsch, Fermi-liquid, non-Fermi liquid, and Mott phases in iron pnictides and cuprates, Phys. Rev. B **81**, 054513 (2010).

[7] A. Liebsch and H. Ishida, Correlation-induced spin freezing transition in FeSe: A dynamical mean field study, Phys. Rev. B **82**, 155106 (2010).

[8] P. Werner, M. Casula, T. Miyake, F. Aryasetiawan, A. J. Millis, and S. Biermann, Satellites and large doping and temperature dependence of electronic properties in hole-doped $BaFe_2As_2$, Nat. Phys. **8**, 331 (2012).

[9] L. Huang and P. Werner (unpublished).

[10] M. Capone, M. Fabrizio, C. Castellani, and E. Tosatti, Strongly Correlated Superconductivity and Pseudogap Phase near a Multiband Mott Insulator, Phys. Rev. Lett. **93**, 047001 (2004).

[11] M. Capone, M. Fabrizio, C. Castellani, and E. Tosatti, Modeling the unconventional superconducting properties of expanded A_3C_{60} fullerides, Rev. Mod. Phys. **81**, 943 (2009).

[12] Y. Nomura, S. Sakai, M. Capone, and R. Arita, Unified understanding of superconductivity and Mott transition in alkali-doped fullerides from first principles, Sci. Adv. **1**, e1500568 (2015).

[13] K. Steiner, S. Hoshino, Y. Nomura, and P. Werner, Long-range orders, and spin/orbital freezing in the two-band Hubbard model, Phys. Rev. B **94**, 075107 (2016).

[14] E. Pavarini, I. Dasgupta, T. Saha-Dasgupta, O. Jepsen, and O. K. Andersen, Band-Structure Trend in Hole-Doped Cuprates and Correlation with $T_{c\max}$, Phys. Rev. Lett. **87**, 047003 (2001).

[15] A. I. Lichtenstein and M. I. Katsnelson, Antiferromagnetism and d-wave superconductivity in cuprates: A cluster dynamical mean-field theory, Phys. Rev. B **62**, R9283 (2000).

[16] G. Kotliar, S. Y. Savrasov, G. Pálsson, and G. Biroli, Cellular Dynamical Mean Field Approach to Strongly Correlated Systems, Phys. Rev. Lett. **87**, 186401 (2001).

[17] T. Maier, M. Jarrell, T. Pruschke, and M. H. Hettler, Quantum cluster theories, Rev. Mod. Phys. **77**, 1027 (2005).

[18] H. Shinaoka, Y. Nomura, S. Biermann, M. Troyer, and P. Werner, Negative sign problem in continuous-time quantum Monte Carlo: Optimal choice of single-particle basis for impurity problems, Phys. Rev. B **92**, 195126 (2015).

[19] A. Georges, G. Kotliar, W. Krauth and M. J. Rozenberg, Dynamical mean-field theory of strongly correlated fermion systems and the limit of infinite dimensions, Rev. Mod. Phys. **68**, 13 (1996).

[20] P. Werner and A. J. Millis, Hybridization expansion impurity solver: General formulation and application to Kondo lattice and two-orbital models, Phys. Rev. B **74**, 155107 (2006).

[21] P. Werner, A. Comanac, L. de' Medici, M. Troyer, and A. J. Millis, Continuous-Time Solver for Quantum Impurity Models, Phys. Rev. Lett. **97**, 076405 (2006).

[22] P. Werner, R. Sakuma, F. Nilsson and F. Aryasetiawan, Dynamical screening in La_2CuO_4, Phys. Rev. B **91**, 125142 (2015).

[23] H. Hafermann, K. R. Patton, and P. Werner, Improved estimators for the self-energy and vertex function in hybridization-expansion continuous-time quantum Monte Carlo simulations, Phys. Rev. B **85**, 205106 (2012).

[24] Despite the orbital-dependent bandwidths, the Mott transition is not an orbital-selective one [2]. This remains unchanged even when we include a realistic crystal-field splitting.

[25] The suppression of low-energy spectral weight is weaker for the c electron than for the f electron. The average of the two spectra yields the local spectral function of the original Hubbard model, with suppressed, but finite, low-energy spectral weight in the weak-doping regime.

[26] A. V. Pimenov, A. V. Boris, L. Yu, V. Hinkov, T. Wolf, J. L. Tallon, B. Keimer, and C. Bernhard, Nickel-Impurity-Induced Enhancement of the Pseudogap of Cuprate High-T_c Superconductors, Phys. Rev. Lett. **94**, 227003 (2005).

[27] S. S. Kancharla, B. Kyung, D. Sénéchal, M. Civelli, M. Capone, G. Kotliar, and A.-M. S. Tremblay, Anomalous superconductivity and its competition with antiferromagnetism in doped Mott insulators, Phys. Rev. B **77**, 184516 (2008).

[28] J. Kunes, Excitonic condensation in systems of strongly correlated electrons, J. Phys.: Condens. Matter **27**, 333201 (2015).

[29] A. Kaminski, S. Rosenkranz, H. M. Fretwell, J. C. Campuzano, Z. Li, H. Raffy, W. G. Cullen, H. You, C. G. Olson, C. M. Varma, and H. Höchst, Spontaneous breaking of time-reversal symmetry in the pseudogap state of a high-T_c superconductor, Nature (London) **416**, 610 (2002).

[30] M. J. Lawler, K. Fujita, J. Lee, A. R. Schmidt, Y. Kohsaka, C. K. Kim, H. Eisaki, S. Uchida, J. C. Davis, J. P. Sethna and E. Kim, Intra-unit-cell electronic nematicity of the high-T_c copper-oxide pseudogap states, Nature (London) **466**, 347 (2010).

[31] Y. Li, V. Baledent, N. Barisic, Y. Cho, B. Fauque, Y. Sidis, G. Yu, X. Zhao, P. Bourges, and M. Greven, Unusual magnetic order in the pseudogap region of the superconductor $HgBa_2CuO_{4+\delta}$, Nature (London) **455**, 372 (2008).

[32] S. Sidis and P. Bourges, Evidence for intra-unit-cell magnetic order in the pseudo-gap state of high-T_c cuprates, J. Phys.: Conf. Ser. **449**, 012012 (2013).

[33] C. M. Varma, Theory of the pseudogap state of the cuprates, Phys. Rev. B **73**, 155113 (2006).

[34] H. Shinaoka, M. Dolfi, M. Troyer, and P. Werner, Hybridization expansion Monte Carlo simulation of multiorbital quantum impurity problems: Matrix product formalism and improved sampling, J. Stat. Mech.: Theory Exp. (2014) P06012.

[35] H. Shinaoka, E. Gull, and P. Werner, Continuous-time hybridization expansion quantum impurity solver for multiorbital systems with complex hybridizations, arXiv:1609.09559.

[36] A. Gaenko *et al.*, Updated core libraries of the ALPS project, arXiv:1609.03930 (2016).

[37] R. K. Bryan, Maximum entropy analysis of oversampled data problems, Eur. Biophys. J. **18**, 165 (1990).

[38] See https://bitbucket.org/lewinboehnke/maxent.

[39] E. Gull, P. Werner, X. Wang, M. Troyer, and A. J. Millis, Local order and the gapped phase of the Hubbard model: A plaquette dynamical mean-field investigation, Europhys. Lett. **84**, 37009 (2008).

[40] E. Gull, O. Parcollet, and A. J. Millis, Superconductivity and the Pseudogap in the Two-Dimensional Hubbard Model, Phys. Rev. Lett. **110**, 216405 (2013).

[41] K. Inaba and S.-I. Suga, Superfluid State of Repulsively Interacting Three-Component Fermionic Atoms in Optical Lattices, Phys. Rev. Lett. **108**, 255301 (2012).

[42] L. Fanfarillo and E. Bascones, Electronic correlations in Hund metals, Phys. Rev. B **92**, 075136 (2015).

[43] A. Liebsch and H. Ishida, Temperature and bath size in exact diagonalization dynamical mean field theory, J. Phys.: Condens. Matter **24**, 053201 (2012).

[44] P. Werner, E. Gull, O. Parcollet, and A. J. Millis, Two-stage metal-insulator transition in the 2D Hubbard model: Momentum selectivity in the 8-site dynamical cluster approximation, Phys. Rev. B **80**, 045120 (2009).

[45] E. Gull, O. Parcollet, P. Werner, and A. J. Millis, Momentum-sector-selective metal-insulator transition in the eight-site dynamical mean-field approximation to the Hubbard model in two dimensions, Phys. Rev. B **80**, 245102 (2009).

[46] L. de' Medici, G. Giovannetti, and M. Capone, Selective Mott Physics as a Key to Iron Superconductors, Phys. Rev. Lett. **112**, 177001 (2014).

[47] M. Ferrero, P. S. Cornaglia, L. De Leo, O. Parcollet, G. Kotliar, and A. Georges, Valence bond dynamical mean-field theory of doped Mott insulators with nodal/antinodal differentiation, Europhys. Lett. **85**, 57009 (2009).

[48] A. F. Albuquerque *et al.*, The ALPS project release 1.3: Open-source software for strongly correlated systems, J. Magnetism Magnetic Mater. **310**, 1187 (2007).